Model for negative-ion extraction, acceleration, and beam transport

C. Michaut
Laboratoire de Physique des Milieux Ionisés, Laboratoire du Centre National de la Recherche Scientifique, Ecole Polytechnique, 91128 Palaiseau Cedex, France
(Received 1 December 1993)

The results of computer simulation of negative-ion extraction, acceleration, and transport are compared to experimental results. The negative ion and electron trajectories are calculated taking into account the potentials applied to the electrodes and the total space charge. The effect of negative-ion stripping and of various atomic collisions are taken into account. In the transport region the space charge includes the effect of positive ions produced by gas ionization. It is shown that the simulation of the accelerator only, with the extrapolation of the results through the transport region, does not reproduce the experimental observations. The simulation including both the accelerator and transport region correctly reproduces the variation of the negative-ion current with acceleration voltage.

PACS number(s): 41.75.Cn, 41.85.−p, 52.20.−j, 02.70.−c

I. INTRODUCTION

Negative ion extraction, acceleration and transport are studied with an experimental setup named INCA (Ions Négatifs: Création et Accélération) at Ecole Polytechnique (Palaiseau). For the need of comprehension of the observed effects, a negative-ion beam computer code has been developed. Two negative-ion extraction computer codes have been developed earlier. There is an early version of Whealton's code [1] and the second one is Pamela's code [2]. They originate from adapting a positive-ion model, therefore, they consider only two species in the plasma source and they calculate only one species trajectories. We will designate them as "positive-ion" models. In the case of negative-ion extraction, electrons are also extracted and their space-charge contribution is between 1% and 4% of the negative-ion space charge. We preferred to develop another code with three plasma species and trajectory calculations for two species. Three plasma species have been considered before in specific negative ion models [3]. To be realistic, more recently these three component models have been considered in full three-dimensional (3D) geometry. The inconvenience of running all simulations in these 3D models, especially when the electron contribution is from 0.5% to 4%, has resulted in most simulations neglecting electrons and run in the 2D approximation [4–6].

The present code also calculates first-order effects of the plasma dynamic in the transport region used in the present experiments and the effects of beam optics in the transport region on the interpretation of the experiments. (A zero dimensional model of positive-ion generation and escape is presented using the actual negative-ion-beam flow and gas densities.) The net positive-ion density is then computed and combined with the negative-ion density through the Poisson equation to calculate modified negative-ion-beam optics due to the altered space charge. However, the treatment is in first order and not self-consistent because the secondary positive ions do not get to sense the effects of the negative-ion space charge. So such well-known phenomena as positive-ion trapping are neglected. The treatment can be expected to give an upper bound for such a phenomenon as "ion focusing."

Negative-ion stripping and charge exchange are considered in the present model in a similar way as in the "positive-ion" models (e.g., Ref. [7]). Negative-ion stripping was also included in Pamela's model [2].

The largest difficulty in effecting the electron extraction calculation is the determination of the density and distribution function of the electrons in the presheath region where some electrons are even in guiding center motion. The local transport, magnetic fields, trapping by the plasma electrode, and highly coupled presheath electric fields are difficult subjects which delay adequate modeling of this plasma. In addition, with one singular instance not considered here is the problem completely in 3D with dominant forces present in the azimuthal direction.

We have chosen to present a simplified model where a convenient model for the electron distribution function is considered and all the aspects of the problem, with the exception of the electron velocities, are treated in 2D. This model neglects azimuthal space-charge forces and the concomitant nonlinear rms emittance growth of the beam. However, we hope that the model will be an improvement over the technique of simply modifying the negative-ion space charge by approximating the mean electron-negative ion departure distance (a single species model). It will certainly not be accurate and reliable if the electron space charge is high; but in the present series of the experiments the density of the electrons is only a few percent of the ion density.

We compare our simulation with our experimental results. Our sources operate with a positive plasma electrode bias, where the H^- ion current is maximum [8,9]. Note that this operating range of the plasma electrode bias is different in other sources [e.g., Culham [10] and Japan Atomic Energy Research Institute (JAERI) [11] sources].

II. GENERAL DESCRIPTION OF THE COMPUTER CODE

A. Principles of development

We developed a simulation code for an H^- beam, but we can easily translate these algorithms for a deuterium ion beam or a beam of another element. The principle of calculation is a particle in cell code in two and a half dimensions: the particle positions are in two-dimension cells, marked by two coordinates (r,z) and the particle velocities are established in the three cylindrical directions (v_r,v_θ,v_z). Thus all the calculation is in a cylindrical revolution symmetry. The ion beam produced by our experimental setup, INCA, is a dc beam, also all temporal physical dependences in the calculation are zero. Each trajectory represents a fictitious tube which is filled up with negative ions. The ions are distributed in the corresponding tube, between the beginning and the end of the trajectory. The temporal continuity is simulated by a spatial continuity of the particle distribution, in the electric-field direction.

The ion and electron trajectories are calculated taking into account the electric field produced by the electrodes, the magnetic field created by permanent magnets, and the electric-field correction due to the space charge. However, the space charge is modified by different collisions of the fast beam particles on the slow background gas particles. For example, fast negative ions are transformed into fast atoms or fast positive ions after collisions with slow hydrogen molecules or atoms. Thus, the total negative charge in the beam decreases and in the same time the positive charge increases. Moreover, the background gas can be ionized by beam particle collisions, which thus reduce the space-charge value.

The calculation proceeds in the following two steps. First, the code treats the ion beam formation in the accelerator and in a small part of the transport region, taking into account the acceleration and pressure conditions. Second, the simulation continues in the whole transport region with the results obtained for the last part of the acceleration region as initial conditions for the transport region. Thus, a small part of the transport region is simulated twice. This is imposed by the choice of the iterative method (boundary potentials are fixed). The same algorithms are used for the calculations in the transport region as for the calculations in the acceleration region.

The code can treat many accelerator types. The user should know very precisely the electrode geometry. Moreover, he must impose as initial conditions, the maximum negative-ion current density, and the thermal energies of the three plasma species: negative ions, positive ions, and electrons.

B. Iterative computational method

The code is based on an iterative method. Figure 1 presents its organization. The user gives all geometry data as potentials and frontiers. The plasma characteristics have also to be imposed by the user. These characteristics are the temperatures of the three species and the extracted negative-ion current. Moreover, the pressures in the source and in the transport region should also be

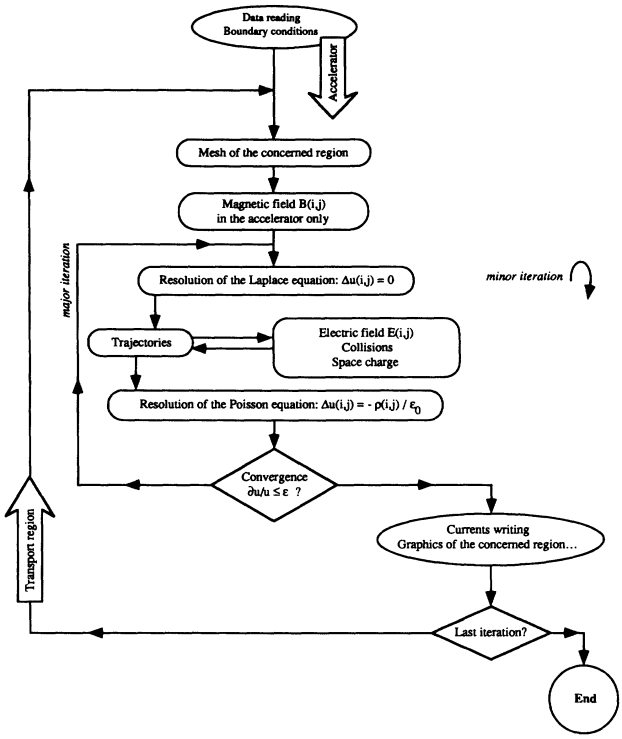

FIG. 1. Schematic organization of the negative-ion-beam simulation code.

indicated.

First of all, the mesh step dimension is calculated to ensure a sufficient accuracy of the calculation. We separate clearly the calculation in two regions, because the mesh accuracy necessary to obtain the computation stability is much smaller near the plasma than in the transport region. First the code treats only the accelerator region including a small part of the transport region (one or two centimeters). When all the accelerator trajectories are stable, the transport region calculation can begin. The results obtained for the last part of the acceleration region are taken as initial conditions for the transport region. Therefore, the trajectories on the first centimeters of the transport region are simulated twice; this is a good way to decrease the effect of fixing the potential of the acceleration region boundary.

Each mesh point has a code number which describes the point situation: in an electrode, in the source plasma, the accelerator or the transport region. In the electrodes and in the source plasma the potentials are known and fixed by the initial conditions. In the beam region, the potentials are unknown and are determined by Poisson's equation. At the beginning, the Poisson's equation is linearized using the finite differences in five points. Then we solve the linearized equation by an iterative method based on the Gauss-Seidel method with overrelaxation. These iteration are called *minor* iterations by opposition to the *major* iterations. A *major* iteration consists of a beam trajectory starting: the potential is calculated on the all mesh points taking into account the beam space charge. The electric field is modified everywhere, thus, the major iteration can start.

The trajectories are launched in the considered

configuration one by one, each one explicitly independently of the others. To make a trajectory, we must accumulate the particle steps succeeding the ones to the others. For each particle step, we must calculate the local acceleration, the particle velocity, and then give a small displacement to this particle. During each step, we have estimated the space charge created by this group of particles and we have dispatched this space charge on the four mesh points of the current cell. The way to dispatch the space charge is also called *cloud in cell.* Consequently, at each trajectory step we have to take into account the collisions which can modify the projectile charge or the target charge. The collisions which are considered are the negative-ion stripping and the background gas ionization.

III. MODELS INTRODUCED IN THE CODE

A. Plasma treatment

We consider three plasma charged particle species: the electrons, the negative ions, and the positive ions. Two simplifying hypothesis have been done: (a) to consider only one positive-ion species in the plasma, namely, H_3^+, because it is probably the majority positive species at the pressures of interest here [12–14]; (b) to attribute a Maxwellian velocity distribution to each plasma population. The maximum negative-ion current density is indicated by the user, it will be noted $J^-_{\max}$. Now, the code has to determine the densities of the three plasma species and the plasma potential.

If $J^-_{\max}$ is known, the initial negative-ion density is defined from the following equation, which corresponds to the experimental findings [15]:

$$J^-_{\max}=en_0^-\left[\frac{kT^-}{2\pi m^-}\right]^{1/2} . \tag{1}$$

The two other densities are estimated from the following two relations:

$$n_{e0}\approx 10n_0^- \ , \quad n_0^+=n_0^-+n_{e0} . \tag{2}$$

The electron density at the center of the extraction region of the source is chosen to be approximately ten times higher than the negative-ion density, as it was found in the experiments [16]. Measurements made in configurations similar to ours support this assumption. The positive-ion density is then obtained from the quasineutrality condition in the source center.

The plasma potential is estimated by considering the equality of the negative and positive charge fluxes at the source wall which is at the potential u_w. Therefore, we write the following equation:

$$\Phi_{w+}=\Phi_{w-}+\Phi_{w^e} , \tag{3}$$

with the flux expressions:

$$\Phi_{w^+}=n_0^+\left[\frac{kT^+}{2\pi m^+}\right]^{1/2} ,$$
$$\Phi_{w^-}=n_0^-\left[\frac{kT^-}{2\pi m^-}\right]^{1/2} e^{e(u_w-u_p)/kT^-} , \tag{4}$$

and

$$\Phi_{w^e}=n_{e0}\left[\frac{kT_e}{2\pi m_e}\right]^{1/2} e^{e(u_w-u_p)/kT_e} .$$

We can neglect the negative-ion flux with respect to the electron flux because of (a) comparable thermal energies, with the electron mass being much lower than the negative-ion mass, and (b) the electron density being taken ten times larger than the negative-ion density. Thus, considering $\Phi_{w^+}=\Phi_{w^e}$ and $n_0^+\approx n_{e0}$, the plasma potential is:

$$u_p=u_w+\frac{kT_e}{2e}\ln\left[\frac{m^+kT_e}{m_ekT^+}\right] . \tag{5}$$

B. Effect of plasma electrode on the electron density

The electron current extracted from the plasma depends directly on the plasma density just in front of the plasma electrode. Both the plasma electron density in front of the plasma electrode and the extracted electron current decrease when the plasma electrode is biased more positive with respect to the source walls. This is related to the fact that the plasma region in front of the plasma electrode is magnetized. We introduced in our code a simple mathematical model to reproduce the influence of the plasma electrode bias on the particle density. This model [17] assumes a potential barrier in front of the plasma electrode. Its results are consistent with the experimental results [9].

The slow plasma electrons move towards the plasma border by diffusion across the transverse magnetic field. The following relation describes the electron current density:

$$j_e=-eD_\perp\nabla n_e . \tag{6}$$

Here, $D_\perp$ represents the transverse diffusion coefficient in the magnetic field. The electron density gradient is

$$\nabla n_e=\frac{n_{e1}-n_{e0}}{L} . \tag{7}$$

Here, L is the thickness of the magnetized zone, n_{e0} is the electron density in the plasma center ($\approx 10n_0^-$) and n_{e1} is the electron density close to the plasma sheath which has to be taken into account at the beginning of the code calculations. Let us denote S the total area of the biased plasma electrode and s the area of the plasma electrode aperture. The extracted electron current is determined as follows:

$$I_{\text{extr}}=en_{e1}\left[\frac{kT_e}{2\pi m_e}\right]^{1/2} s . \tag{8}$$

The electron current collected by the plasma electrode itself, denoted I_b, is

$$I_b=en_{e1}\left[\frac{kT_e}{2\pi m_e}\right]^{1/2} Sf(V_b-u_p) . \tag{9}$$

The function $f(V_b-u_p)$ describes the potential barrier created in front of the plasma electrode when it is nega-

tively biased with respect to the plasma potential u_p. We write this function as follows:

$$f(V_b-u_p)=\begin{cases}\exp\left[\dfrac{V_b-u_p}{T_e}\right] & \text{if } V_b<u_p \\ 1 \text{ if } V_b>u_p\ .\end{cases} \tag{10}$$

The total electron current is the sum of the extracted current and of the current collected by the plasma electrode: $I_e=I_{\text{extr}}+I_b=j_e(S+s)$. From this equality, the electron density value n_{e1} in front of the extraction aperture is obtained:

$$I_e=en_{e1}\left[\frac{kT_e}{2\pi m_e}\right]^{1/2}s+en_{e1}\left[\frac{kT_e}{2\pi m_e}\right]^{1/2}Sf(V_b-u_p)$$

$$=-eD_\perp\frac{n_{e1}-n_{e0}}{L}[s+Sf(V_b-u_p)]\ . \tag{11}$$

Then,

$$n_{e1}=n_{e0}\left[\frac{1}{1+\left[\dfrac{kT_e}{2\pi m_e}\right]^{1/2}\dfrac{L}{D_\perp}\dfrac{s+Sf(V_b-u_p)}{s+S}}\right]\ . \tag{12}$$

The $L/D_\perp$ ratio is not known exactly, it is a parameter which can be fitted to experimental results. Figure 2 presents the variation of the calculated extracted electron current versus the plasma electrode bias, for several values of the parameter $L/D_\perp$ and compares it to an experimentally found dependence for I_{extr}.

C. Simple and double stripping of H^- ions

The two main reactions undergone by the negative-ion beam are as follows (with their cross-section notation): The simple electron stripping is

$$\underline{H^-}+H_2\ (\text{or H})\Longrightarrow\underline{H^0}+H_2\ (\text{or H})+e^-\ \ (\sigma_{-10}) \tag{13a}$$

and the double-electron stripping is

$$\underline{H^-}+H_2\ (\text{or H})\Longrightarrow\underline{H^+}+H_2\ (\text{or H})+2e^-\ \ (\sigma_{-11}) \tag{13b}$$

Here we underline the fast particles which are the collision projectiles. As there are two kinds of the particle targets in the background gas (hydrogen atoms and molecules), we have to take into account four types of collisions in the calculation.

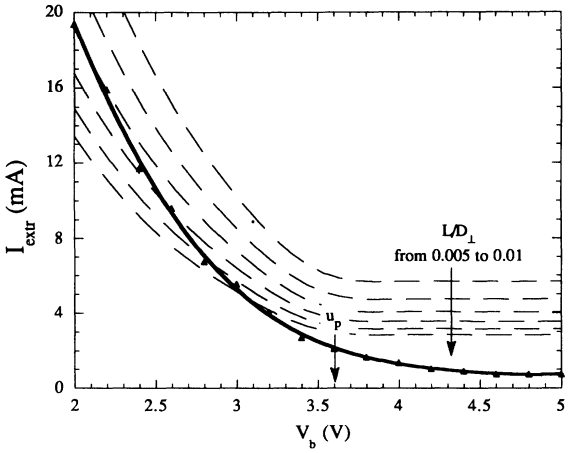

FIG. 2. Variation, versus the plasma electrode bias V_b, of the calculated electron current extracted from the source plasma, for several values of the parameter $L/D_\perp$. The measured extracted electron current (full triangles and full line) is also shown.

Usually the double-electron stripping is negligible before the simple electron stripping at the considered beam energy, because the cross section σ_{-10} is approximately ten times larger than σ_{-11}. But positive-ion creation in the transport region is very important for the beam focusing [18]. As we use the same algorithm in the two regions, we take into account everywhere the positive-ion formation induced by the double-electron stripping.

The cross sections are calculated for all the incident particle energies by a Chebyshev orthogonal polynomials T_i method balanced by the parameters A_i adjusted for each cross section [19]. The cross section is calculated by the following relation:

$$\sigma(E)=\exp\left[\frac{A_0}{2}+\sum_{i=1}^{8}A_iT_i(X)\right], \tag{14}$$

with

$$X=\left[\ln\frac{E}{E_{\min}}+\ln\frac{E}{E_{\max}}\right]\Big/\ln\frac{E_{\max}}{E_{\min}}\ .$$

When a negative-ion fraction is transformed to neutrals or positive ions, the space charge $\rho(r,z)$ must be modified. For the negative-ion orbits, we solve during each small displacement the following equation:

$$\frac{dn^-}{dl}=-n^-[n_{H_2}(\sigma_{-10}+\sigma_{-11})|_{H_2}+n_H(\sigma_{-10}+\sigma_{-11})|_H]\ . \tag{15}$$

Since the longest jump is chosen sufficiently small for the energy to be constant and for the change in reaction rate to be always very low, we can write the density after a small displacement k, respectively, for the negative ions $\underline{H^-}$, the neutrals $\underline{H^0}$, and the positive ions $\underline{H^+}$:

$$n_k^-=n_{k-1}^-(1-[n_{H_2}(\sigma_{-10}+\sigma_{-11})|_{H_2}+n_H(\sigma_{-10}+\sigma_{-11})|_H]\partial l)\ , \tag{16}$$

$$n_k^0=n_{k-1}^-[n_{H_2}\sigma_{-10}|_{H_2}+n_H\sigma_{-10}|_H]\partial l\ , \tag{17}$$

$$n_k^+=n_{k-1}^-[n_{H_2}\sigma_{-11}|_{H_2}+n_H\sigma_{-11}|_H]\partial l\ . \tag{18}$$

D. Ionization of background gas

All the particles extracted from the source plasma acquire very soon after their extraction enough energy to ionize the background gas. Therefore, we should consider three charge states of the beam particles and the also the fast electrons. These electrons are extracted from the source and are deflected in the magnetic field produced by four permanent magnets contained in the extraction electrode. We have to consider four reactions occurring with two possible target particles (hydrogen atoms and molecules), so we have eight reactions and their respective cross sections.

$$\text{Ionization by electrons: } \underline{e^-}+H_2 \text{ (or H)} \Rightarrow \underline{e^-}+H_2^+ \text{ (or } H^+)+e^- \quad (\sigma_i|_{e^-}) ; \tag{19}$$

$$\text{ionization by } H^-\text{: } \underline{H^-}+H_2 \text{ (or H)} \Rightarrow \underline{H^-}+H_2^+\text{(or } H^+)+e^- \quad (\sigma_i|_{H^-}) ; \tag{20}$$

$$\text{ionization by } H^0\text{: } \underline{H^0}+H_2 \text{ (or H)} \Rightarrow \underline{H^0}+H_2^+ \text{ (or } H^+)+e^- \quad (\sigma_i|_{H^0}) ; \tag{21}$$

$$\text{ionization by } H^+\text{: } \underline{H^+}+H_2 \text{ (or H)} \Rightarrow \underline{H^+}+H_2^+\text{(or } H^+)+e^- \quad (\sigma_i|_{H^+}) . \tag{22}$$

Since all the phenomena taken into account in the calculation are stationary, because in the experiment the plasma production and the beam formation are dc, the equilibrium between the production and the loss of the slow positive ions has to be found. So we use again a simple mathematical model to account for the positive-ion creation and loss [20].

For example, the instantaneous H_2^+ production due to H^- collisions on the molecules H_2 is described by the following equality:

$$\frac{dN(H_2^+)}{dt}=N(H_2)n(H^-)\sigma_i|_{H^-}v^- . \tag{23}$$

The H_2^+ ions are lost because they leave the volume inside which they were created. They are inevitably produced in the projectile impact surface. Each orbit has its own impact surface noted S, depending on the initial radial distance of the given orbit. The ion production volume per unit time is $V=Sv^-$. The loss surface is $\Sigma=Lv^-$, where L is the surface S contour. Hence, the H_2^+ loss through this creation volume border and by time unit gives the leaving ion flux:

$$\frac{dN(H_2^+)}{dt}=N(H_2^+)v^+\frac{Lv^-}{Sv^-} . \tag{24}$$

The number of H_2^+ ions in this volume is determined by equating the H_2^+ production and loss rates [Eqs. (22) and (23)], and is as follows:

$$N(H_2^+)=N(H_2)n(H^-)\sigma_i|_{H^-}\frac{v^-}{v^+}\frac{S}{L} . \tag{25}$$

The movement of the energetic negative ions and the slow molecular positive ions in the volume occupied by the negative ions of the same orbit, during one second, is represented schematically on Fig. 3. The volume length is determined by the H^- velocity.

The positive-ion movement depends on their creation place. In the transport region, their velocity is close to the one of molecules before ionization, while the positive ions formed in the accelerator are under the influence of very strong potential gradients. Their energy can be ten thousand times larger than that of H_2^+ ions in the transport region. Therefore, their contribution to the space charge is much less important in the accelerator than in the transport region.

We know now the positive-ion density created by H^- collisions on the background gas along an H^- orbit in the transport region. When the pressure in the transport region is increased, the number of collisions with the background gas increases and more fast negative ions are transformed into neutrals H^0, or into positive ions H^+. Since the cross sections of these two charge-changing collisions are of the same order of magnitude and the number of energetic neutrals and positive ions increases when the number of negative ions decreases, we have to consider them in the calculation of the positive-ion production. In order to estimate the H_2^+ ion density due to the collisions of the energetic neutrals and positive ions, on the particles of the background gas, we assume that the energetic neutrals and positive ions continue their motion with the same velocity and in the same direction as their H^- parent ions. This approximation would be completely justified, if all the negative-ion trajectories were perfectly straight.

We count in the meantime and using the same method the slow H^+ ions created by the beam particle collisions on the atoms in the transport region. We remind the reader that the source gas flux contains around 10% of hydrogen atoms. In this calculation, we consider four different pressure regions going from the source to the

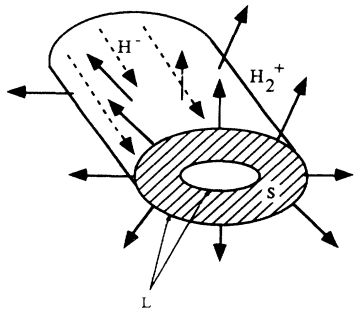

FIG. 3. Illustration of the movement of the energetic negative ions and slow molecular positive ions in the volume occupied by the negative ions of the same orbit, during one second. The volume length is determined by the H^- velocity.

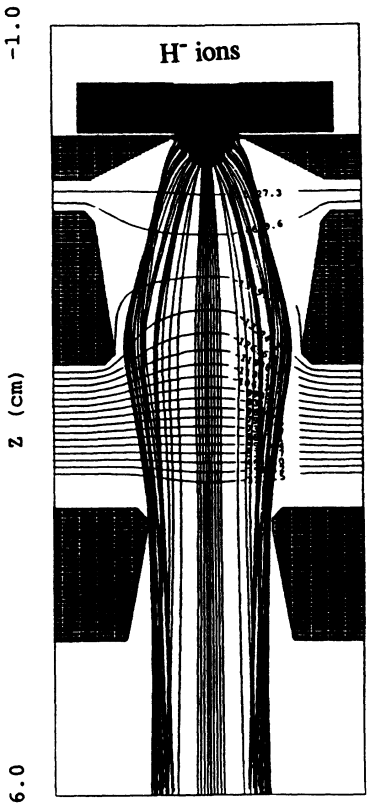

FIG. 4. Calculated negative-ion trajectories.

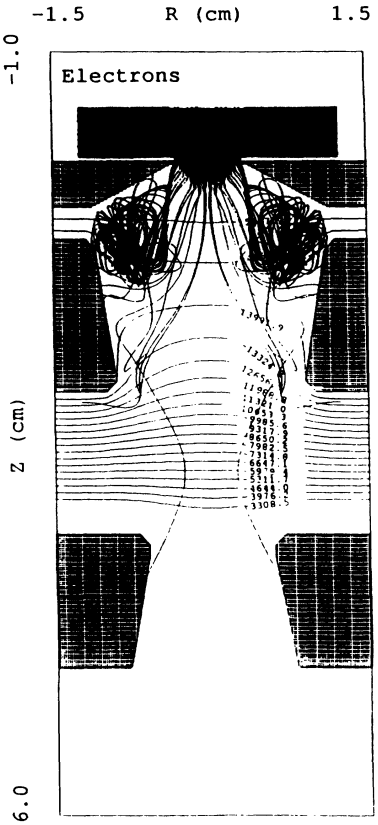

FIG. 5. Calculated electron trajectories.

transport region, of which only the source pressure and the transport region pressure are known [18]. The two intermediate pressures are calculated considering the opening conductances. For example, if the source pressure is 5 m Torr and the transport region pressure is 7×10^{-2} m Torr, the two intermediate pressures are, respectively, 2.2 m Torr and 3×10^{-1} m Torr.

Figure 4 presents the trajectories of negative ions obtained by simulation, while Fig. 5 presents the electron trajectories.

IV. VALIDATION BY EXPERIMENT

Early so-called "positive-ion codes" gave results for negative-ion extraction which were mostly unsuccessful even in the prediction of the maximum accelerator perveance [21]. Attempts at modeling more specific to negative-ion extraction has led to the result [5], which for the first time made agreement with negative-ion accelerator perveance. Using this same analysis, which for this example ignores electrons, and makes no nontrivial account of the transport, gives significant disagreement with the new data [22]. To come towards agreement, resort had to be made to inclusion of positive ions generated in the electron trap (not included in the present analysis). The present analysis agrees with the present data without including the backstreaming positive ions in the acceleration region, but including the electron effect and the transport beam optics (which has no effect on the perveance as will be seen in what follows).

A. Extraction voltage experiments

To focus the beam in the Faraday cup, we have to simultaneously optimize the extraction and acceleration voltages. On Fig. 6 we show the dependence of the negative-ion-beam current upon the extraction voltage, V_{extr}. At each V_{extr}, the acceleration voltage, V_{acc}, was optimized to obtain the maximum negative-ion current in

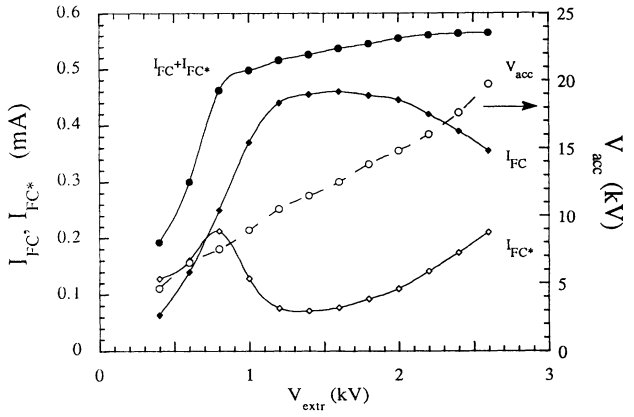

FIG. 6. Dependence of the H^--ion current to the Faraday cup and its front plate upon the extraction voltage. The sum of these two currents is also shown. The optimum acceleration voltage is also presented (open circles). Plasma electrode bias: $V_b=3.2$ V. $P_{trans}=8.6\times10^{-2}$ m Torr. Plasma electrode opening diameter: $\Phi_{PE}=0.65$ cm.

the Faraday cup (I_{FC}). We also plot on Fig. 6 the optimum acceleration voltage versus V_{extr}. Note that the dependence of optimum V_{acc} on V_{extr} is linear and that I_{FC} is maximum when V_{extr} is in the range 1.2–1.8 kV. The negative current to the Faraday cup front plate FC* (a ring with the outer diameter 10 cm) is minimum when I_{FC} is maximum. Thus, there is only a narrow range of V_{extr} in which the negative ion beam is focused. Figure 6 shows also that the sum of the mentioned two currents, $I_{FC}+I_{FC^*}$, continues to increase when V_{extr} increases. We can suppose that the total density of the extracted negative ions increases with V_{extr}, and the negative beam space charge increases. In conclusion, the beam becomes too divergent to be focused in the Faraday cup when V_{extr} becomes higher than the optimum extraction voltage.

Nightingale and Holmes reported that the negative-ion beam can be focused on a target with any value of the extraction voltage, but with a constant ratio between the acceleration and the extraction voltages [23]. They underline that this phenomenon is specific to negative-ion-beam formation. We saw on Fig. 6, that for a given plasma there is only one optimum extraction voltage. But, if we were measuring only the total negative-ion current ($I_{FC}+I_{FC^*}$), we would have also concluded that all the extraction voltages can focus the beam. The plasma sheath physics is not the same in the case of positive-ion-beam extraction and negative ion-beam extraction. In the latter case, the plasma electrons, extracted in the meantime as the negative ions, have a considerable action on the sheath shape when the electron space charge in the sheath is comparable to the negative-ion space charge.

Whealton *et al.* made numerical simulations of the bending out of the plasma sheath due to the ion extraction [5]. They observed the shift of the sheath, dependent on the applied extraction voltage.

We simulated two cases with our numerical simulation code. The first case is for a low V_{extr} and the second one is for a strong V_{extr} with respect to the optimum one. Figure 7 shows the shift of the plasma-beam frontier. The plasma sheath is materialized by the equipotential u_p+1 V, it is drawn by the dotted line on the Fig. 7. We observe that this line is displaced by the change of the extraction voltage.

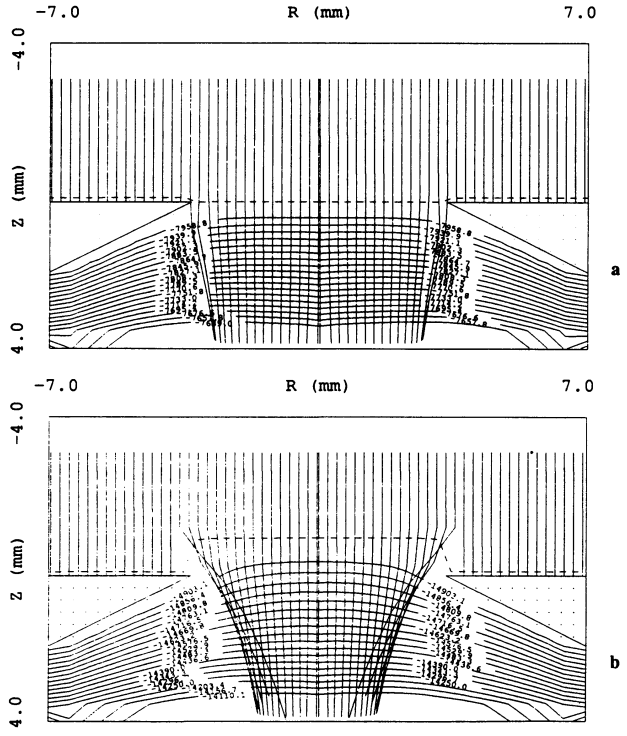

FIG. 7. Simulation of potential distributions in the extraction region for two different extraction electrode voltages. (a) represents a low extraction voltage: $V_{extr}=1$ kV, $V_{acc}=8$ kV, while (b) represents a higher extraction voltage: $V_{extr}=4$ kV, $V_{acc}=15$ kV. Plasma electrode bias: $V_b=5$ V. Plasma potential is $u_p=3.6$ V. The diameter of the plasma electrode opening is $\Phi_{PE}=0.65$ cm.

B. Acceleration voltage experiments

The beam particles reach the full energy at the level of the third electrode, which we designate as the acceleration electrode. In Sec. IV A we showed that there is an optimum extraction voltage, for which an acceleration voltage can be chosen to maximize the current to the Faraday cup. Figure 8 presents the beam current variation versus the acceleration voltage, for two different extraction openings in the plasma electrode. The extraction voltage was constant in the two measurements shown.

Note that the Faraday cup current I_{FC} increases abruptly starting from approximately 8 kV, attains a maximum value, and then decreases very quickly when the acceleration voltage is increased. The ring current I_{FC^*}, which is the H^--ion current reaching the Faraday cup front plate, increases starting from a very low acceleration voltage, attains a maximum before decreasing when I_{FC} starts going up. Then it increases again at higher acceleration energy. These successive variations reflect the beam focusing in the Faraday cup due to the adjustment of the acceleration voltage (V_{acc}). This demonstrates that there is only one acceleration voltage to correctly focus the beam, when all the other source and accelerator parameters are fixed.

The experiment of Fig. 8(a) has been simulated and is presented on Fig. 9. Two different calculations are shown: (1) the calculation is effected in the accelerator only and is extrapolated through the transport region (dotted lines); (2) a complete calculation, i.e., accelerator and transport region, drawn with full lines and full symbols.

Note that the complete simulation, i.e., including both the accelerator and the transport region, corresponds rather well to the experiment. We insist on the fact that the simulation in the accelerator only is not sufficient. In general, the effect of the transport region cannot be obtained by simply extrapolating the accelerator region results. In the presented case, the transport region pressure (6.5×10^{-2} m Torr) is close to the optimum pressure (7×10^{-2} m Torr), therefore, the difference between the

two simulation procedures is not very important yet. This is because at optimum pressure the beam space charge in the transport region is low, the beam being approximately neutral.

The effect of the pressure in the transport region has also been studied experimentally. The simulation has correctly reproduced the observed variation of the negative-ion-beam current with the mentioned pressure [18], the beam focusing at high pressure, and the beam space-charge expansion, at low pressure. We have found that there is an optimum transport pressure for improved a beam optics and maximum negative-ion current. For multiple applications of negative-ion beams a good beam optics in the transport region is essential. Therefore, our result suggests to suitably choose the pressure in the low-energy beam transport region of particle accelerators. This should also apply to the pressure in front of the neutralizer in fusion neutral injection beam lines.

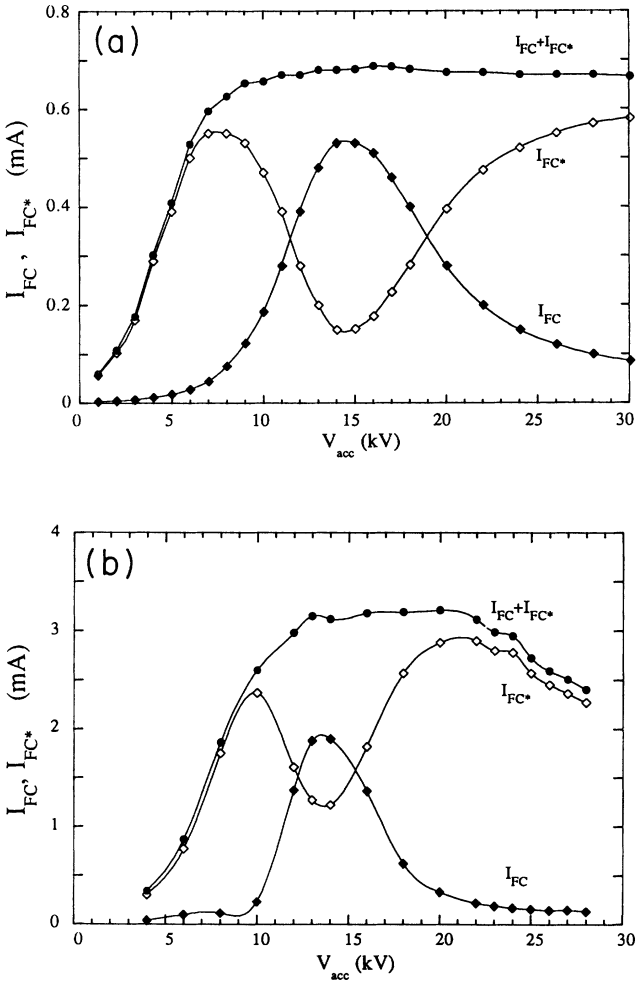

FIG. 8. Dependence of the measured H^--ion current to the Faraday cup and its front plate upon the acceleration voltage. The diameter of the opening in the plasma electrode is 0.65 cm. (a) $V_b=5.0$ V and $V_{extr}=1.9$ kV. $P_{trans}=6.5\times10^{-2}$ m Torr, plasma electrode opening is $\Phi_{PE}=0.65$ cm; (b) $V_b=3.8$ V and $V_{extr}=2.1$ kV. $P_{trans}=2.9\times10^{-2}$ m Torr, plasma electrode opening is $\Phi_{PE}=1.30$ cm.

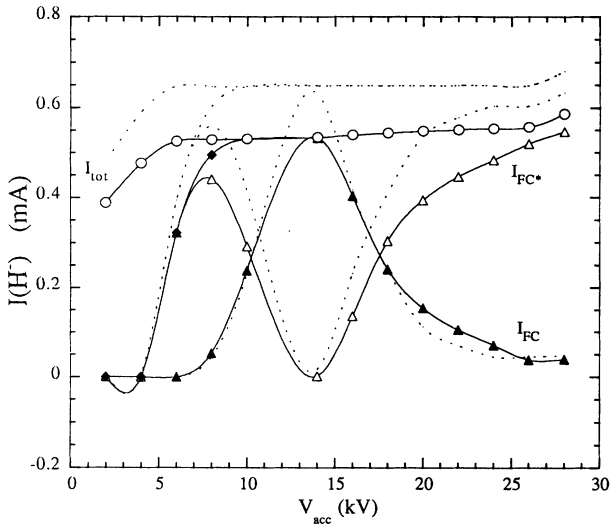

FIG. 9. Simulation of the negative-ion current dependence upon the acceleration voltage. The two other accelerator electrode voltages are kept constant: $V_b=5$ V and $V_{extr}=1.9$ kV. $\Phi_{PE}=0.65$ cm. Transport region pressure: $P_{trans}=6.5\times10^{-2}$ m Torr.

V. CONCLUSION

The present simulation code treats the extraction, the acceleration, and the transport of the negative ions. At first, the calculation is done in the acceleration region. When the stability of this calculation is reached, the trajectories are launched into the transport region. The trajectories are calculated by taking into account the potential gradients imposed by the electrodes and the total space charge.

The trajectories of the electrons extracted from the plasma are also simulated. These electrons can have a dominant role in the space charge near the plasma limit.

In both regions, the code takes into account the negative-ion collisions, which lead to their (simple and double) stripping. Furthermore, in the transport region, the space charge includes the contribution of positive ions formed by gas ionization.

The production of positive ions in the accelerator (by gas ionization) can play an important role. Being accelerated towards the plasma, they enter into it and certainly modify the shape of the sheath [18]. We plan to take into account this effect in the simulation code. In order to improve the model of the plasma produced in the transport region, we should have simulated the movement of the slow positive ions. In its present state, the code has accounted for the beam gas focusing in the transport region, at high pressure, and for the beam blowup, when the pressure in the transport region is low [22]. These effects, demonstrated by the simulation, are in agreement with our experiments.

We have studied numerically the effect of each of the three electrodes of our accelerator. The conclusions, thus obtained, corroborate our observations. In particular, our code correctly predicts the dependence of the

currents to the Faraday cup and its front ring, without including the backstreaming positive ions in the accelerator region, mainly by including the transport region. Due to this initial achievements, we plan to further develop this code, along the above-mentioned lines.

ACKNOWLEDGMENTS

Useful discussions with Dr. J. H. Whealton, Dr. T. Mihail, Dr. J. Bruneteau, and Dr. M. Bacal are acknowledged.

[1] J. H. Whealton, M. A. Bell, R. J. Raridon, K. E. Rothe, and P. M. Ryan, J. Appl. Phys. **64**, 6210 (1988).
[2] J. Paméla, Rev. Sci. Instrum. **62**, 1163 (1991).
[3] J. H. Whealton, P. S. Meszaros, R. J. Raridon, and K. E. Rothe, Rev. Sci. Instrum. **61**, 436 (1990).
[4] C. Michaut, P. Devynck, M. Bacal, Z. Sledziewski, F. P. G. Valckx, J. H. Whealton, and R. J. Raridon, Rev. Sci. Instrum. **63**, 2774 (1992).
[5] J. H. Whealton, P. S. Meszaros, R. J. Raridon, K. E. Rothe, M. Bacal, J. Bruneteau, and P. Devynck, Rev. Phys. Appl. **24**, 945 (1989).
[6] J. H. Whealton, M. A. Bell, R. J. Raridon, K. E. Rothe, and P. M. Ryan, J. Appl. Phys. **64**, 6210 (1988).
[7] R. J. Raridon, J. H. Whealton, J. W. Wooten, R. W. McGoffey, D. E. Wooten, and C. C. Tsai, J. Appl. Phys. **57**, 819 (1985).
[8] C. Michaut-Béhar, Thèse de doctorat de l'Université Paris VI; PMI Report No. 2779, 1993 (unpublished).
[9] M. Bacal, J. Bruneteau, and P. Devynck, Rev. Sci. Instrum. **59**, 2152 (1988).
[10] A. J. T. Holmes, G. Dammertz, and T. S. Green, Rev. Sci. Instrum. **56**, 1967 (1985).
[11] Y. Okumura, H. Horiike, T. Inoue, T. Kurashima, S. Matsuda, Y. Ohara, and S. Tanaka, in *Production and Neutralization of Negative Ions and Beams,* Proceedings of the Fourth International Symposium on the Production and Neutralization of Negative Ions and Beams, Brookhaven, 1986, edited by James G. Alessi, AIP Conf. Proc. No. 158 (AIP, New York, 1986), p. 309.
[12] A. M. Bruneteau, Thèse de doctorat ès sciences physiques, Université de Paris–Sud; PMI Report No. 1310, 1983 (unpublished).
[13] K. N. Leung, R. D. Collier, L. B. Marshall, T. N. Gallahar, W. H. Ingham, R. E. Kribel, and G. R. Taylor, Rev. Sci. Instrum. **49**, 321 (1978).
[14] E. Nicolopoulou, M. Bacal, and H. J. Doucet, J. Phys. (Paris) **38**, 1399 (1977).
[15] R. Leroy, M. Bacal, P. Berlemont, C. Courteille, and R. A. Stern, Rev. Sci. Instrum. **63**, 2686 (1992).
[16] M. Bacal, A. M. Bruneteau, and M. Nachman, J. Appl. Phys. **55**, 15 (1984).
[17] J. Bruneteau, in *Proceedings of the 2nd European Workshop, 1986 Palaiseau, France,* edited by M. Bacal and Chantal Mouttet (Ecole Polytechnique, Palaiseau, 1986), p. 81.
[18] C. Michaut and M. Bacal, Rev. Sci. Instrum. **65**, 1424 (1994).
[19] C. F. Barnett, *Atomic Data for Fusion,* ORNL Publ. No. 6068 (ORNL, Oak Ridge, TN, 1990), Vol. 1.
[20] W. J. Lichtenberg, K. Bethge, and H. Schmidt-Bocking, J. Phys. B **13**, 343 (1980).
[21] Besides Ref. [7], this includes subsets, namely, the SNOW, WOLF, KOBRA, AXCEL, BEAM, and ARGUS codes.
[22] R. G. Cowan, J. Niemel, R. L. Campbell, R. J. Raridon, J. H. Whealton, C. Michaut, and M. Bacal, in *Production and Neutralization of Negative Ions and Beams,* Sixth International Symposium, Upton, NY, 1992, edited by James G. Alessi and Ady Hershcovitch, AIP Conf. Proc. No. 287 (AIP, New York, 1992), p. 621.
[23] M. P. S. Nightingale and A. J. T. Holmes, Rev. Sci. Instrum. **57**, 2396 (1986).